The Influence of LO Power Heating of the Tunnel Junction on the Performance of THz SIS Mixers

Alessandro Traini , Boon-Kok Tan , John D. Garrett , Andrey Khudchenko , Ronald Hesper ,
Andrey M. Baryshev, Pavel N. Dmitriev, Valery P. Koshelets , and Ghassan Yassin

Abstract—We describe the performance of a superconductor–insulator–superconductor (SIS) mixer operating in the frequency range of 780–950 GHz. Unlike most SIS mixers, the tunnel junction employs two different superconductors, a niobium nitride top and a niobium bottom electrode sandwiching an aluminum nitride barrier layer, fabricated on a niobium titanium nitride ground plane. The mixer was tested in a pulse tube cryostat, with all the optical components, in the signal path, mounted inside the vacuum environment to avoid attenuation of the RF signal as it propagates from the hot/cold loads to the mixer. With this setup, we have measured an RF-corrected noise temperature of ∼220 K. In this article, we focus on investigating the influence of local oscillator (LO) power heating on the performance of the terahertz mixer. The increase in the junction's physical temperature can be observed experimentally by noting the suppression of the gap voltage in the pumped current–voltage (I–V) curve as the LO pumping level is increased. Similar observation has already been reported, and attempts were made to estimate the effective temperature of the device using equations of heat transfer between the mixer chip layers. Here, we present an experimental method of quantifying this effect by recovering the effective temperature of the junction through comparing the pumped I–V curves at different pumping levels and fixed bath temperature, with the unpumped I–V curves obtained at varying bath temperatures. We also estimate, for the first time, the effect of heating on the noise temperature as a function of bath temperature and frequency. We show that for typical experimental parameters, the LO heating can increase the double-sideband receiver noise temperature by as much as 20%, and that in the frequency range of the measurements, the effective temperature of the junction at fixed LO power increases linearly with frequency at a rate of 0.5 K/100 GHz.

Index Terms—Heating effect, superconductor–insulator–superconductor (SIS) junctions, SIS mixers, terahertz (THz) mixers.

I. INTRODUCTION

IN RECENT years, there has been increasing interest in extending the frequency coverage of millimeter and sub-millimeter telescopes beyond the 1-THz threshold [1]. This is because the atmospheric transmission at good dry sites such as the Chajnantor plateau would allow astronomical observations in windows centered at 1.3 and 1.5 THz. These frequency windows contain important astronomical information that can be obtained by observing a host of spectral line emission by CO, NH+, and other molecules [2] to probe the dense core and structure of molecular clouds where star formation took place [3]. The Herschel Space Observatory has already detected the lowest energy rotational transitions of ND [4] at frequencies above 1 THz, but there is still the need to interpret the absence of NH+ in the same portion of the band and to understand the chemistry of the star-forming clouds. Detecting molecular hydrogen lines with the Atacama Large Millimeter/Submillimeter Array (ALMA) in the frequency range 1.2–1.6 THz (known as Band 11) would allow direct detection of the redshifted H$_2$ emission [5] from galaxies at a redshift z∼10, yielding detailed measurements of evolved stars photosphere and direct evidence of the active galactic nucleus feedback in the early universe. In addition to that, observations beyond 1 THz will bring more insight into a broad range of science cases, including the intermediate redshifted universe [6], protoplanetary disks [7], extragalactic sources [8], and the cosmic infrared background [9].

While astronomical receivers using all-Nb tunnel junctions can perform well at frequencies up to ∼1 THz [10]–[12], the performance starts to deteriorate rapidly as the frequency approaches 1.3 THz. This is because the photon step structure in the pumped voltage–current (I–V) curve is suppressed as the pump frequency exceeds twice the gap frequency. Efforts to develop superconductor–insulator–superconductor (SIS) mixers with higher gap superconductors such as niobium nitride (NbN) or niobium titanium nitride (NbTiN) are ongoing, but so far the realization of an SIS mixer using all-NbN or NbTiN tunnel junctions that is suitable for astronomical receivers at THz
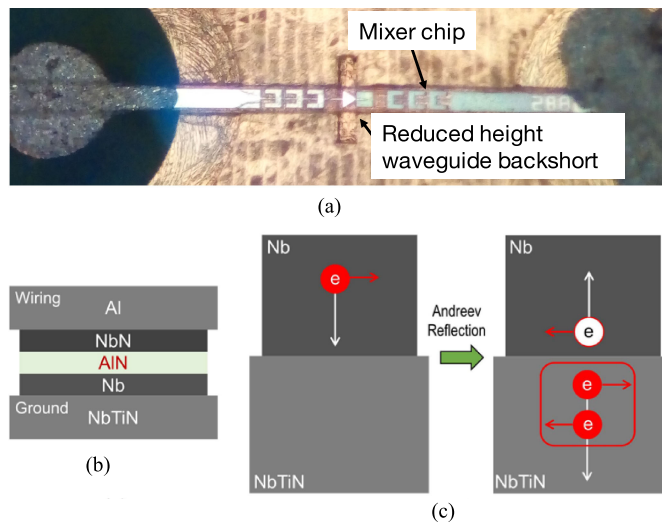
(a)

(b)

(c)

Fig. 1. (a) Image showing the mixer chip used in our experiment. (b) Schematic geometry of the SIS tunnel junction used in this experiment, along with the superconducting material used to form the ground and wiring layer of the mixer circuit. (c) Boundary between the Nb and the NbTiN ground plane presents a gap discontinuity, where the quasi-particle current can flow through the interface via the process of Andreev reflection.

Fig. 2. Suppression of the gap voltage due to the LO heating. The I–V curves are measured at a constant bath temperature of 4 K.

frequencies remains illusive. A successful solution to circumvent this is to use a hybrid junction, for which Nb is deposited as a bottom electrode and a higher gap superconductor is deposited as a top electrode [13], [14]. For example, employing NbN as the top electrode ($T_c \sim 16$ K) would produce an energy gap high enough to be suitable for employment at supra-THz frequencies.

Another important consideration in designing a high-frequency mixer is the choice of materials used for realizing the superconducting circuit. Nb films are extremely lossy above the gap frequency and, hence, should be replaced by either a higher gap superconductor or normal metal. Both options have different pros and cons that are beyond the scope of this article. Nevertheless, it is worth noting that a lot of care needs to be taken in designing circuits for a supra-THz SIS mixer, that is low loss and broad band while keeping the size of the junction and the dimensions of the transmission lines used in these circuits feasible for fabrication.

II. HYBRID JUNCTION AND LOCALIZED HEATING EFFECT

The geometry of the mixer chip used in our experiment is shown in Fig. 1. The tunnel junction comprises a Nb/AlN/NbN trilayer fabricated on a NbTiN ground plane with the aluminum (Al) normal metal forming the top wiring layer.[1] Although it has been shown previously that operating such a device as a heterodyne mixer is possible [14], the employment of a hybrid junction that comprises multiple superconductors with different superconducting gaps can give rise to heating of the tunnel junction when coupled to the power of a strong local oscillator (LO) source, degrading the noise performance of the mixer.

[1]It would of course be better to replace the Al layer by either NbN or NbTiN film. However, this method seems to degrade the performance of the tunnel junction considerably.
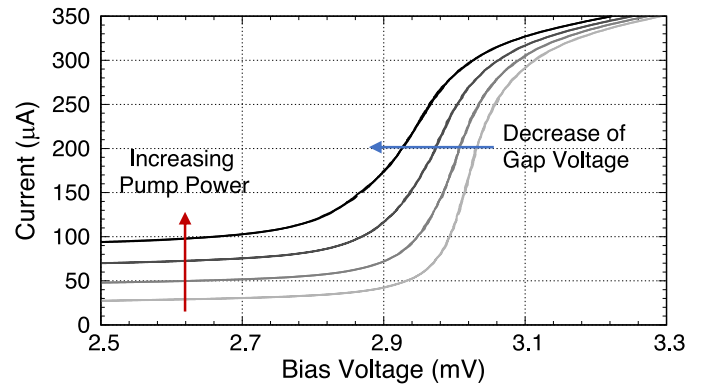
This effect is observed experimentally as the superconducting gap voltage in the pumped I–V curve is reduced notably when the mixer is injected with a strong LO power, and the gap suppression increases with pump level, as shown in Fig. 2.

To explore the cause of heating, we shall first consider the transport of charge across a tunnel junction that uses ground plane or wiring layer materials with superconducting gaps higher than those employed by the tunnel junction itself. In a junction that uses a sandwich of identical superconductors, and the same material for the wiring and ground plane layers, the energy deposited by the LO is transported out by the tunneling quasi-particle current flowing across the electrodes. In our device, however, the energy gap of the NbTiN ground plane is higher than the Nb bottom electrode of the junction. As a result, the tunneling quasi-particle current flowing from the Nb electrode to the NbTiN ground plane encounters an energy step that impedes the current's energy transport. Consequently, the quasi-particles on the lower gap superconductor can only move across the boundary via Andreev reflection by creating a Cooper pair in the high-gap superconductor, resulting in the reflection of a hole in the lower gap superconductor, as shown in Fig. 1(c). This process is allowed as it conserves energy and momentum of the tunneling quasi-particles, but it could leave the thermal energy trapped at the boundary and, therefore, heats the tunnel junction locally. The Andreev reflection alone, however, cannot explain the strong dependence of the heating on the LO power in our junction, nor it can explain the fact that our measured pumped I–V curves were completely symmetrical with respect to the direction of the junction bias current. In fact, while Andreev reflection is needed for current transport in our device in a particular bias direction, it may not cause any heating, since the reflected hole by the Nb/NbTiN energy step can escape away from the device by tunneling back and recombining with an electron in the Al electrode. This is in contrast to the process in junctions that use high-gap superconductors for both the wiring and ground plane layers, since Andreev reflection in that case is symmetrical and occurs for electrons at one interface and for holes at the other [15].

A possible explanation for the LO heating has already been proposed [14] and was attributed to the resistive properties of the

junction materials. For example, Nb, which has an energy gap well below the photon energy, can show resistance to current in the frequency range of our measurements. In fact, gap suppression can be observed in the I–V curves of the ALMA Band 10 devices with all-Nb junctions, although at much lower level than in our device [11], [12]. Significant gap voltage suppression can also be seen in reported pumped I–V curves of a supra-THz SIS mixer using an all-Nb tunnel junction [10]. We would also like to note that the NbN film may have also contributed to the resistive behavior of our device, since the critical temperature of our junction was estimated at ∼9.9 K (see Section V). This makes the transition temperature of this film about 10.8 K, which translates to a superconducting gap frequency of about 820 GHz.

The problem of heat trapping in SIS tunnel junctions has already been investigated theoretically [15]–[20], and attempts were made to calculate the effective temperature of the quasi-particles using the heat transfer equation between the junction and the substrate. While the results of these calculations gave reasonable estimates of the device's effective temperature (T_{eff}), it was difficult to find accurate values as a result of the uncertainty in choosing the correct power law index in the heat transfer equation and in estimating the electron–phonon interaction time for different materials.

In this article, we present an experimental method for finding the effective temperature T_{eff}. This is done by comparing the gap voltage (V_g) of a series of pumped I–V curves at varying pump levels and fixed bath temperature (T_b), with a series of unpumped I–V curves at varying T_b between 3 and 6 K. In this way, we are able to recover T_{eff} from the experimental data, and in the process, we demonstrate that the gap suppression does indeed occur as a result of LO heating. In addition to calculating T_{eff}, we also investigated the influence of heating on the noise temperature of the THz mixer in the frequency range 800–900 GHz. Measurement of the mixer's noise temperature as a function of LO power has shown that the heating effect degrades the mixer performance substantially. We further verified that, as expected, the noise contribution of the RF components between the device and the input loads is not affected by the LO heating.

III. THz SIS Mixer

The design of the THz SIS mixer used in this experiment has been reported in detail previously [14]; hence, we will only briefly summarize the mixer's properties. The mixer chip uses two high-current-density (30 kA/cm²) 0.5-μm² SIS tunnel junctions separated by an inductive microstrip section to tune out the mixer junction capacitance over a broad bandwidth. A triangular probe was used to couple the RF/LO signals to the mixer junction. The mixer chip was mounted across the narrow channel of a reduced height rectangular (75 × 300 μm) waveguide with the probe laying in the E-plane. Both the ground plane and the wiring layer were terminated by RF chokes to prevent the RF signal from leaking to the intermediate frequency (IF) circuit, as shown in Fig. 1(a). The superconducting circuit was fabricated on a 40-μm-thick quartz substrate and mounted in a back-piece with the normal vector to the chip aligned with the direction of propagation of the incoming RF/LO waves. The

back-piece was then aligned with the rectangular waveguide of the feed horn's circular to rectangular transition and were both held together using a threaded centering ring. This assembly (back-piece/horn) was slotted into a mixer block that has the same layout as the ALMA Band 9 block [21], but modified for operation in the frequency range of 780–950 GHz.

The original ALMA Band 9 mixer assembly employed a corrugated horn followed by a circular-to-rectangular waveguide transition electroformed in a single metal block. However, to avoid the complexity of milling tiny corrugations and electroforming, we replaced the corrugated horn by a smooth-walled horn, which was fabricated by direct drilling of the feed into a block of aluminum followed by a circular-to-rectangular waveguide transition, also fabricated by direct milling. The performance of the smooth-walled horn has already been reported [22], [23] and was shown to have comparable performance to that of a corrugated horn in a similar frequency range. We would like to emphasize, however, that the back-piece carrying the mixer chip was connected to a half-height waveguide of 75 × 300 μm, while the horn's circular-to-rectangular waveguide transition was fabricated with a full-height rectangular waveguide of 150 × 300 μm, due to the difficulty in direct machining accurately a high-aspect-ratio rectangular waveguide of such small dimensions. This has obviously resulted in a significant mismatch between the two waveguides. To correct for this mismatch in the noise temperature estimation, we modeled the scattering parameters of this discontinuity using Ansys High-Frequency Structure Simulator (HFSS). We found that the mismatch resulted in a loss of ∼16–20% RF power coupling to the SIS devices, which increased the mixer noise temperature substantially, as we will show later.

IV. Experimental Setup and Noise Measurement Results

The mixer characterization was performed in a pulse tube cooler (PTC) system, where the bath temperatures could be controlled within 1 mK during a measurement at a particular temperature. In Fig. 3, we show a schematic view of the cryogenic setup used in this investigation, where the hot and the cold loads used in the Y-factor measurements and the optical components in the RF signal path were mounted inside the cryostat.² A flat copper plate coated with Stycast 2850FT [24] and mounted on the inner side of the cryostat optical window was used as a 300-K blackbody "hot load," while the inner wall of a conical section coated with the same material and bolted to the cold plate was used as a 4 K "cold load." A rotating mirror mounted on top of a cryogenic stepper motor was used to switch the mixer beam between the hot and cold loads. The LO power was coupled to the mixer from outside the cryostat using a Gaussian telescope arrangement, with the collimating mirror positioned in front of an optical window outside the cryostat, and the focusing mirror mounted inside the cryostat close to the mixer feed. Both optical windows were followed by infrared filters mounted on the inner shield stage to reduce the thermal

---

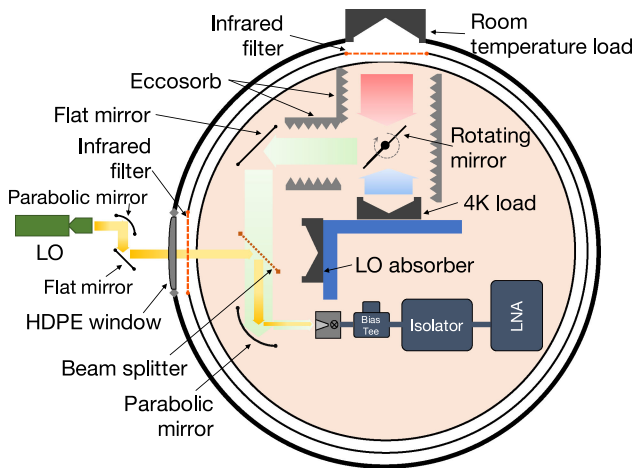²The E-plane is vertical to the direction of propagation.

Fig. 3. Schematic of the cryostat optical arrangement for performing the noise temperature characterization.
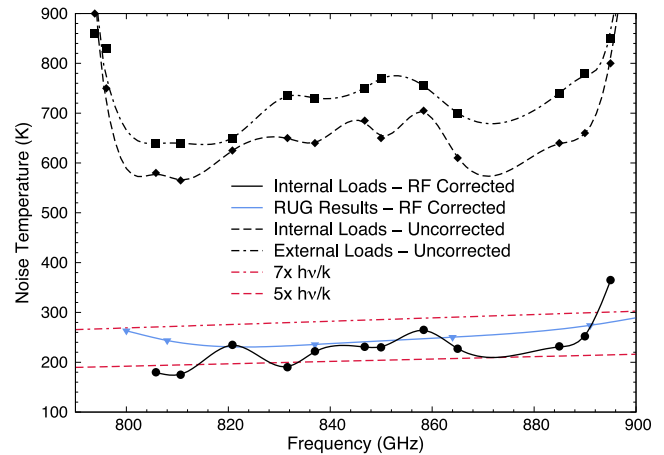

Fig. 4. Comparison of noise temperature curves obtained with different methods. The dashed–dotted–dashed curve represent the result measured with external loads, while the dashed curve shows the uncorrected result measured with internal loads. The black solid curve shows noise temperature with the internal loads, corrected for the RF losses of the waveguide mismatch and beam splitter. The blue solid curve depicts the results measured in another experiment carried out at the Kapteyn Astronomical Institute, corrected for beam splitter loss.

loading of the cryostat. This setup ensured that losses that could have been experienced by an RF signal propagating from the loads outside the cryostat and passing through lossy components across the optical window are eliminated.

The RF and LO beams were combined inside the cryostat using a 19-μm-thick mylar beam splitter mounted on a titanium alloy bracket, with the base attached to the cold plate. We used the titanium alloy to reduce the thermal coupling between the cold plate and the beam splitter, as the mylar tends to expand at cryogenic temperatures. We have experienced this effect in our initial experiments as the sagging of the mylar following cooling distorted the alignment of the beams and the mixer was not at all pumped even at maximum LO power. To prevent the mylar from sagging when it is cooled, the beam splitter was strongly stretched repeatedly through several thermal cycles, which reduced the thickness of the beam splitter to 17 μm.

The PTC cryostat was also equipped with four temperature sensors that were attached to the internal cold blackbody source, the mixer block, the cold plate, and the second-stage shield. The temperature of the cold plate and the second stage could be increased above the minimum values using resistors installed behind these plates. The voltage across the resistors was controlled by a proportional–integral–derivative controller loop, which was set to maintain the temperature of the sensor attached to the mixer block to the desired bath temperature T_b, with an accuracy of ~1 mK (in what follows, the phrase "bath temperature T_b" will be used to indicate the temperature of the mixer block). The capability to accurately control the temperature of the mixer block allowed us to test the mixer at different bath temperatures, which is crucial for a proper characterization of the heating effect. The double-sideband noise temperature of the receiver (often referred to as the "mixer noise temperature") was measured using a standard SIS mixer IF chain in the frequency range of 4–6 GHz, using a cryogenic high-electron-mobility transistor amplifier with a noise temperature of ~5 K.

To verify the integrity of our internal load setup, we initially replaced the room temperature blackbody load mounted on the cryostat window with a "transparent" dielectric window

and fixed the position of the rotating mirror so that the mixer beam was direct toward the cryostat window. In this way, the Y-factor measurement could be performed in the conventional way, by illuminating the mixer with either a room temperature hot load or a 77 K liquid nitrogen cold load, both located outside the cryostat. The comparison between the noise temperature measurements taken with either the internal loads or the external loads is shown in Fig. 4. It can be seen that an improvement of ~100 K in the noise temperature was obtained when the internal loads setup was used, which is consistent with the RF transmission losses induced by the dielectric window and the IF filter, except at 820 GHz, where we suspect that measurement was degraded by enhanced LO noise, giving an inconsistent measurement. The rise in noise temperature at the lower and higher ends of the frequency range was mainly caused by the limited operational bandwidth of our LO source. An added advantage of the internal loads method is that the Y-factor is much larger considering that the cold load is at ~4 K instead of 77 K. We would like to emphasize that calculation of the power emitted by the internal cold blackbody was done using the Callen–Welton equations [25] as the Rayleigh–Jeans approximation, which requires $h\nu/k_B T \ll 1$, where h is Planck's constant, ν is the RF, k_B is the Boltzmann constant, and T is the cold load temperature, is not valid for such a low value of cold load and high RF.

The experimental curves in Fig. 4 show noise temperature values, which are higher than expected when compared with the noise temperature measured for a similar device [14]. This substantial increase in noise temperature is attributed to the mismatch between the full-height waveguide of the feed horn's transition and the half-height waveguide of the back-piece where the mixer chip is mounted. We have, therefore, corrected the RF noise for this mismatch contribution using the data from the HFSS simulation and placing the mismatch as a lossy components in the receiver chain used to calculate the RF noise of the
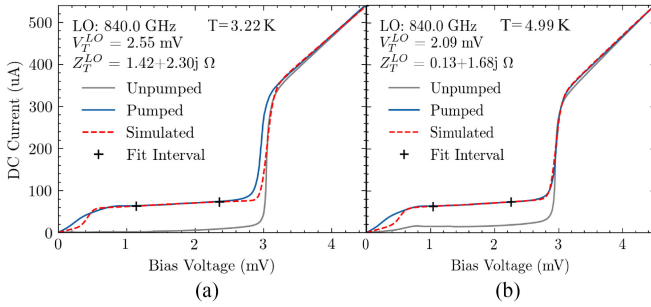
Fig. 5. Recovering the effective temperature T_{eff} of the mixer chip by matching the pumped $I–V$ curve measured at $T_b = 3.22$ K with simulated pumped curves at different T_b values. (a) Simulated $I–V$ curve does not match the pumped $I–V$ curve when calculated at $T_b = 3.22$ K. (b) Simulated curve matches very well the measured pumped $I–V$ curve when calculated at $T_b = 4.99$ K.

Fig. 6. Comparison of the gap voltages V_g of unpumped $I–V$ curves measured at different bath temperatures T_b, with pumped $I–V$ curves measured at different pumping levels. The solid gray–black curves represent the unpumped curves, while the dashed pink–red represent the pumped curves.

mixer. We also corrected for the noise contribution of the beam splitter by first measuring the transmission as a function of frequency using a Fourier transform spectrometer (approximately 82% transmission) and inserting an equivalent component in the receiver chain. As expected, the correction of the RF noise contribution reduced the noise temperature significantly, since the influence of the RF losses is cascaded down the receiver chain. The corrected results shown in Fig. 4 are now close to $5 \times$ the quantum limit and consistent with the results obtained in a separate experiment performed at the Kapteyn Astronomical Institute, University of Groningen (RUG). Note that we did not include the atmospheric absorption in our comparison (atmospheric loss is ~2–3% per meter in our frequency range) because when measurements were done with external loads, the hot and cold loads were held at a distance of 1–2 cm from the cryostat window.

V. LO HEATING EFFECT

In this section, we focus on the effect of the LO power heating on the tunnel junction and how it may influence the performance of the SIS mixer. We first studied the effect of LO heating by comparing simulated pumped $I–V$ curves using unpumped $I–V$ curves at different bath temperatures with the experimental pumped $I–V$ curve measured at a fixed T_b. The simulated $I–V$ curves were obtained from the following relation:

$$I_0(V_b) = \sum_{n=-\infty}^{\infty} J_n^2(\alpha) I_{\text{dc}}(V_b + n\hbar\omega/e) \qquad (1)$$

where the pump factor $\alpha = V_{\text{LO}}/\hbar\omega$ is calculated from the standard impedance recovery method [26], V_{LO} is the amplitude of the LO voltage across the tunnel junction, V_b is the bias voltage, $J_n(\alpha)$ is the Bessel function of order n, $V_b + n\hbar\omega/e$ is the equivalent voltage when n photons are absorbed, and the rest of the parameters take their usual definition.

The pumped $I–V$ curve we attempted to match in Fig. 5 was measured at 840 GHz with $T_b = 3.22$ K. As can be seen in Fig. 5(a), the simulated pumped curve calculated with an umpumped $I–V$ curve at the actual bath temperature $T_b = 3.22$ K results in a gap voltage, which is significantly higher than that of the measured curve, indicating that the tunnel junction
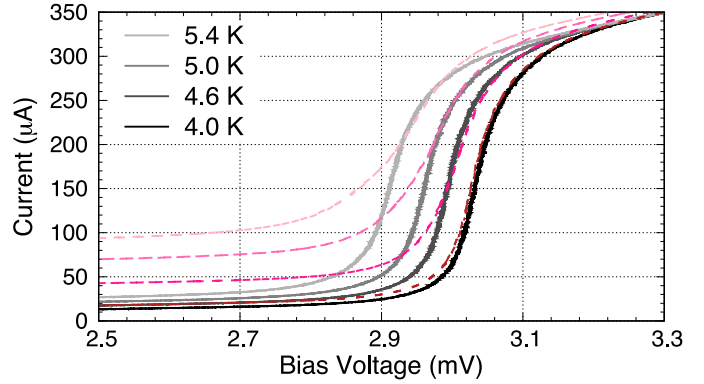
must be operating at a higher effective temperature. And indeed, when the simulated pumped $I–V$ curve was calculated with unpumped curve at $T_b = 4.99$ K, an excellent match to the measured pumped curve was obtained over almost the whole width of the photon step including the shape of the gap, indicating that the effective temperature of the tunnel junction T_{eff} was increased to ~4.99 K when it was pumped with the LO, which is almost 1.8 K higher than the bath temperature.

An alternative way to find the effective temperature T_{eff} is to compare the gap voltages V_g of the experimentally pumped $I–V$ curves with the gap voltages V_g of unpumped $I–V$ curves measured at different bath temperatures T_b. Increasing the LO power or increasing T_b has the same effect of suppressing the gap voltage V_g. This method is simpler as it only employs the experimental data and does not require the complexity of repeated impedance recovery calculation as we reiterate to match a simulated $I–V$ curve to the measured pumped $I–V$ curve. Fig. 6 shows a series of pumped $I–V$ curves, measured at 831 GHz and a bath $T_b = 4.0$ K with varying pump levels, along with a family of unpumped curves measured at varying T_b between 4.0 and 5.4 K. The effective temperature can be read directly by comparing the V_g values of the two sets of curves. For example, the V_g value corresponding to the curve with the second highest pumping level coincides with the V_g of an unpumped curve measured at $T_b = 5.0$ K, while the gap voltage V_g corresponding to the curves with the third highest pumped level matches well the bath temperature of the unpumped curve at $T_b = 4.6$ K.

The determination of the gap voltage V_g and its variation with LO power and bath temperature depends on the choice of the corresponding current point on the different $I–V$ curves to which the values of V_g are referred. We have, therefore, used two different techniques to measure V_g, as shown in Fig. 7, to ensure that our definition of the gap voltage has little influence on the conclusion of our investigation. A straightforward way to determine the values of V_g for a series of $I–V$ curves is to refer the gap values to a fixed current point at the center of the transitions, as shown by the blue dots in Fig. 7. An alternative method, however, is to calculate the gradient of each $I–V$ curve and look for the point of maximum steepness, as shown by the
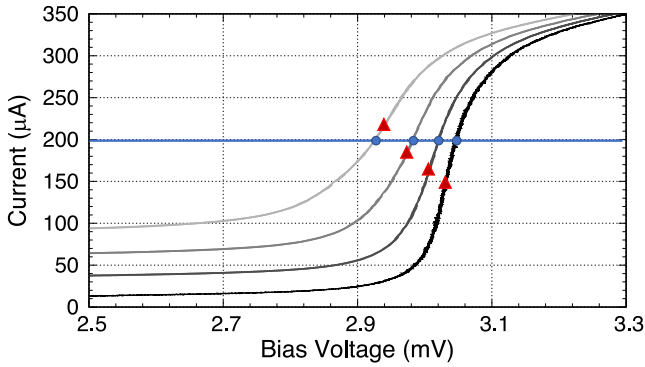
Fig. 7. Plots illustrating the two methods used to determine the gap voltage V_g. The blue dots were measured using the methods that read the gap voltages of the I–V curves at a fixed current value near the center of the transition. The red triangles were obtained using the maximum steepness method. The unpumped I–V curve is plotted in black, while the pumped curves are plotted with gray-shaded curves for different pumping levels.
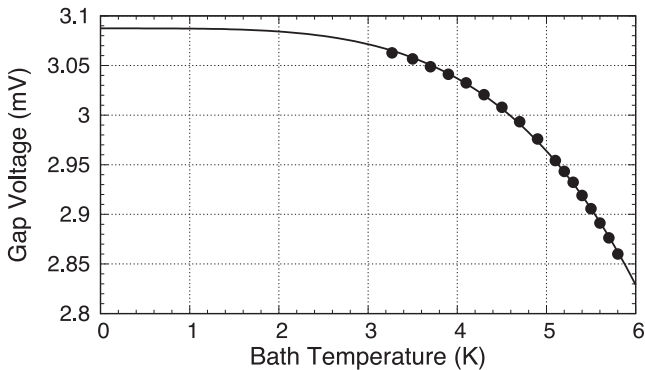

Fig. 8. Gap voltage of the unpumped I–V curves plotted against the bath temperature. The solid curve was calculated using (2), while the measured data were plotted using the circular dots. The best fit of the data gave a gap voltage value at 0 K of 3.09 mV.

red triangles in Fig. 7. The gradient curve gives a more accurate estimation of the middle point across the transition but requires a fast Fourier transform filter to remove the noise in the dataset that could have a steeper gradient than the midpoint of the gap transition. We have compared the two methods in calculating the effective temperature T_{eff} and found that the difference was less than 5% (see Fig. 10).

Another interesting method to verify V_g determination techniques is to plot the measured V_g for a series of unpumped I–V curves as a function of T_b and then compare these data with the theoretical relation for V_g given by the following relation [27]:

$$V_g(T) = V_g(0)\sqrt{\cos\left(\frac{\pi}{2}\frac{T_b^2}{T_c^2}\right)} \qquad (2)$$

where $V_g(0)$ is the gap voltage at the zero temperature and T_c is the critical temperature. The parameters we optimized to best fit the data are the critical temperature T_c and the gap voltage $V_g(0)$. The result given in Fig. 8 shows that the theoretical curve and the measured data match extremely well. Although we used the maximum steepness method to compile the dataset of the V_g values, the difference between the two methods in
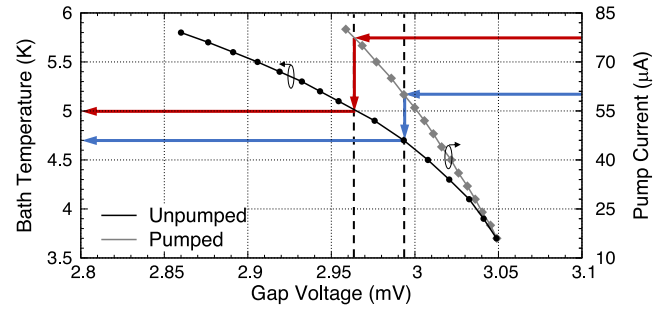

Fig. 9. Plot illustrating how we recover the effective temperature T_{eff} of the device by linking the pump current of the pumped I–V curve to the bath temperature of the unpumped curve. The red and blue arrows show the sequence of how T_{eff} can be read directly from the pump current, for two different pumping levels. The pumped I–V curve was measured at a fixed bath temperature of 3.3 K.

inferring $V_g(0)$ was less than 0.02 mV. We would like to note that the excellent agreement between the measured and calculated values of V_g, as shown in Fig. 8, validates the integrity of our determination of the effect of heating on the gap voltage of the pumped curve and hence the actual temperature of the device. Moreover, it provides an experimental method to find the value of the transition temperature of hybrid junctions. This is a useful technique since the quality of the superconducting film is usually altered when layers of different materials are deposited on top of each other during the fabrication process. In our case, we have measured a critical temperature of $T_c \sim 9.9$ K, which is lower than expected for a Nb/NbN junction but consistent with gap voltage value measured for the unpumped I–V curve.

VI. INFLUENCE ON THE MIXER PERFORMANCE

We have shown above how to recover the effective temperature T_{eff} of the device experimentally by inspecting the gap voltage V_g of the pumped I–V curves and associating it to a bath temperature T_b, using the unpump curve so that $T_{\text{eff}} = T_b$ when the curves cross each other (see Fig. 6). In practice, however, it is much easier to determine T_{eff} from the value of the pump current I_p measured at the center of the photon step. This becomes possible whence the data linking the V_g to the pump current I_p and that data linking V_g to the bath temperature T_b of the unpumped I–V curves are obtained.

In Fig. 9, the black curve plots the relation between V_g and T_b for a set of unpumped I–V curves, while the gray curve gives V_g as a function of varying pumping level I_p when the device is stabilized at a fixed $T_b = 3.3$ K. As an example, if the I_p value for a pumped I–V curve reads 60 μA, then by following the blue arrows, we can infer that $V_g \sim 2.99$ mV, which, in turn, indicates that $T_{\text{eff}} = T_b = 4.7$ K. Similarly, if the device is pumped with stronger LO power, where $I_p = 77$ μA, then by following the red arrows, we find that the devices must have been heated up to 5 K, which is approximately 1.7 K higher than the bath temperature.

We summarize our findings here in Fig. 10 by plotting the dependence of the effective temperature on the LO power level. The gray-shaded curve indicates the small variations in V_g when obtained using the two different techniques we discussed earlier. It can be seen that the effective temperature increases quite
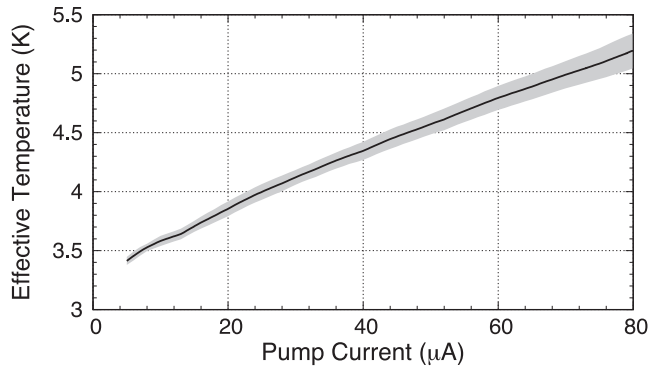
Fig. 10. Equivalent temperature of the junction as a function of the pump current when the device was stabilized at a fixed bath temperature of 3.3 K. The plot was obtained with the device illuminated with an 831-GHz LO signal. The gray-shaded curve represents the variation in T_{eff} data when V_g is estimated using the two different methods discussed earlier.
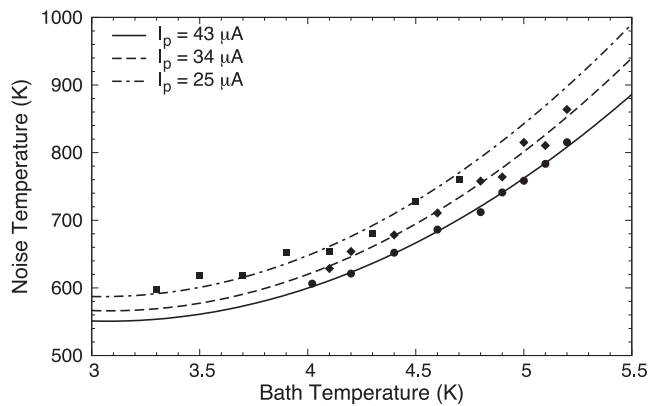

Fig. 11. Measured mixer noise temperature plotted as a function of bath temperature for three different pumping levels. The data were fitted with quadratic curves to guide the eyes.

sharply with the pump current level I_p. Considering that our optimum noise temperature at an LO frequency of 831 GHz was obtained at an LO pump level of $I_p \sim 60\ \mu\text{A}$, we conclude that LO heating (under optimum working parameters) can increase the device temperature by ~ 1.5 K. As we shall see later, this has significant effect on the mixer performance.

In order to investigate the impact of LO heating on the mixer noise temperature (T_N), we have measured T_N as a function of the bath temperature, when the device was injected with three different LO power levels around the optimum level value. The results in Fig. 11 show that the mixer T_N increased by about 20% when the bath temperature was increased from 4 to 5 K, with similar behavior observed at the three pumping levels. It is also interesting to note that further cooling of the mixer reduces the slope of the curve. For example, increasing the bath temperature from 3.3 to 4 K increases the noise temperature by only 9% compared to 20% when the bath temperature was increased from 4 to 5 K. Unfortunately, our cryostat did not allow cooling below 3.2 K, but extrapolating the data to lower bath temperatures shows that T_N is likely to plateau when the mixer is cooled below 3 K, which is $0.3 \times T_c$ (we have shown earlier that the critical temperature of the junction is $T_c \sim 9.9$ K).
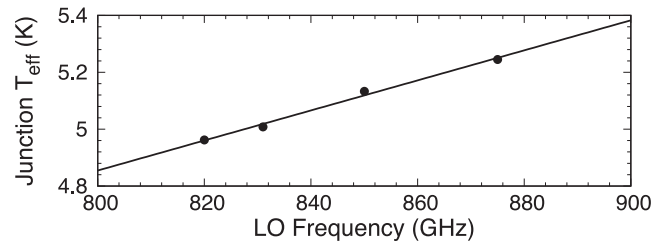

Fig. 12. Equivalent effective temperature of the junction as a function of LO frequency measured at a fixed bath temperature of 4 K and a fixed pump level at $I_p = 60\ \mu\text{A}$. The slope of the black curve is 0.53 K per 100 GHz.

This is an interesting result since cooling to 3 K is within what can be achieved by modern PTC systems. This also indicates that there is an added advantage of using hybrid junctions with higher critical temperatures. For example, increasing the critical temperature of the junction to 12 K guarantees that the LO heating would not degrade the performance of the mixer if it is cooled to a bath temperature of 3.6 K.

The influence of heating was also studied as a function of LO frequency, as shown in Fig. 12. It can be seen that the effective temperature of the junction increases almost linearly with the LO frequency in our measurement frequency range. Here, we have chosen to keep the tunnel junction at the same pump level by ensuring that the pump current I_p remains the same at all frequencies. The increase in T_{eff} can, therefore, be attributed to the fact that higher frequency photons carry more energy. In particular, we find that the equivalent gap temperature increased by 0.53 K when the LO frequency was increased by 100 GHz. If the LO heating increases at a similar rate for higher frequencies, then this result implies that a lot of care must be taken when using hybrid junctions at frequencies above 1 THz, because at supra-THz frequencies, the LO heating can be substantial. For example, if we extrapolate the curve in Fig. 12 to an SIS mixer operating at 1.3 THz, the increase in T_{eff} can be as high as 2.5 K, bringing the junction T_{eff} to about 7.3 K. This is about 74% of the critical temperature of the hybrid junction studied here, which will obviously cause severe degradation of the performance of the SIS mixer.

The contribution of the SIS tunnel junction to the mixer (receiver) noise temperature is done through two mechanisms. The first is through the added noise of the junction (ideally equal to $h\nu/k$) and the second is through the conversion loss of the device, which multiplies the IF contribution in the receiver chain. To investigate the influence of heating on each of these two fundamental properties of the mixer, we first plotted the conversion loss of the mixer as a function of the bath temperature, as shown in Fig. 13(a). It can be clearly seen that the conversion loss increases with increasing T_b across the full measurement range. However, we also note that as the temperature increases from 3.2 to 5 K, the conversion gain decreases from 41% to 30%, which will only cause a small increase in the noise temperature. We, therefore, conclude that the increase in the mixer noise temperature as a result of LO heating comes from the added noise by the tunnel junction, which is cascaded through the lossy components of the receiver as can be seen from the following
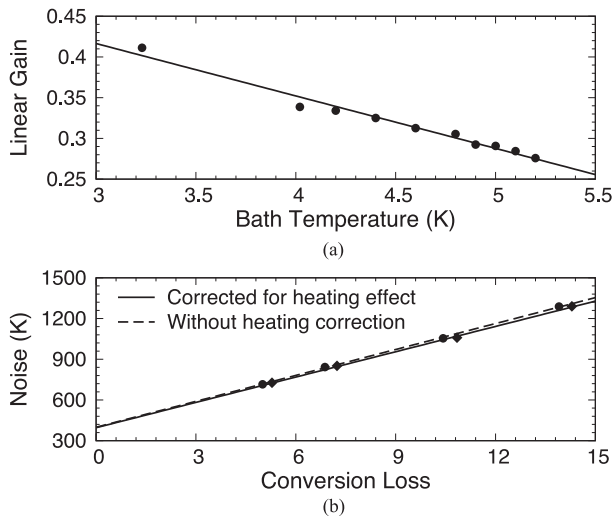
Fig. 13. (a) Mixer gain plotted as a function of the bath temperature. The data were obtained with the LO frequency set to 831 GHz. The black curve is a linear fit to the data with a slope of $-0.064\,\mathrm{K}^{-1}$ and an intersection of 0.6 at $T_b = 0$. (b) RF noise contribution estimated by correcting for the heating effect compared to the uncorrected estimation. The noise temperature correction was calculated with the mixer gain data shown in (a), and the two methods gave very similar values of 399 and 396 K for uncorrected and correction estimation, respectively.

relation:

$$T_N = \left(\frac{1}{G_{\mathrm{RF}}} - 1 \right) T_{\mathrm{RF}} + \frac{T_{\mathrm{SIS}}}{G_{\mathrm{RF}}} + \frac{T_{\mathrm{IF}}}{G_{\mathrm{RF}} G_{\mathrm{SIS}}} \tag{3}$$

where G_{RF} and T_{RF} are the noise temperature and insertion gain of the RF chain between the SIS device and receiver input, respectively, and G_{SIS} and T_{SIS} are the conversion gain and noise temperature of the SIS tunnel junction, respectively. Finally, we will investigate the influence of LO heating on the receiver RF contribution.

Based on the discussion above, we can see that LO heating is localized inside the junction; hence, we expect it to increase the junction added noise [second term in (3)] and the noise of the subsequent IF components in the chain (third term), but not the contribution of the RF components between the device and the receiver input (first term). To verify this assumption, we have calculated and compared the RF noise contribution with and without the LO heating influence. Calculation of the RF noise was done using the well-known modified "interception method" [28], which is implemented by plotting the noise temperature of the mixer as a function of the mixer conversion loss using several LO power levels and searching for the y-intercepting coordinate. This method makes the assumption that the noise temperature of the mixer is insensitive to small changes in the LO power in the linear regime. However, we now know that because of LO heating, this assumption is no longer valid. We have, therefore, made the plot both with and without modifying the noise temperature and mixer gain values by LO heating. Modification of the noise temperature and mixer gain was done as explained above [using Figs. 11 and 13(a)]. Comparison of the two methods is given in Fig. 13(b), which clearly shows that the RF noise contribution is not influenced by LO heating. The RF noise estimated from both datasets is approximately 400 K.

VII. CONCLUSION

We have presented an extensive experimental study of the LO heating effect on the hybrid Nb/AlN/NbN tunnel junctions fabricated between a NbTiN ground plane and an Al wiring layer, in the frequency range of 800–900 GHz. Measurements were made in a THz receiver with the optics in the RF path and the loads used to measure the Y-factor located inside the cryostat. To test the advantages of the internal optics system, we measured the noise temperature of the mixer and obtained a value of about 220 K, in good agreement with measurements made at the RUG. We have then investigated the influence of the LO heating of the tunnel junction on the performance of the SIS mixer. This was done by using the experimental data to calculate the junction effective temperature as a function of both the LO power and the LO frequency. We have found that the degradation of the mixer noise temperature by the heating effect depends strongly on the mixer physical temperature. This was illustrated by the fact that the noise temperature of the mixer increased by 20% as the bath temperature increased from 4 to 5 K. Extrapolation of our experimental data to lower temperature reveals that the LO heating effect becomes negligible at bath temperatures below 3 K, which is approximately $0.3 \times$ the transition temperature of our junction. We have also found that the effective temperature of the tunnel junction at fixed pump level increases sharply with LO frequency with a slope of about 0.5 K/100 GHz. This indicates that the heating by the LO power can substantially degrade the performance of a supra-THz SIS mixer employing hybrid junctions, operating at liquid helium bath temperatures. The influence of heating, however, can be reduced by cooling the mixer below $0.3 T_c$, which is feasible using modern PTCs.

REFERENCES

[1] D. Rigopoulou *et al.*, "Science with ALMA band 11 (1.0–1.6 THz)," *Messenger*, vol. 153, pp. 35–37, 2013.
[2] E. Herbst and E. F. Van Dishoeck, "Complex organic interstellar molecules," *Annu. Rev. Astron. Astrophys.*, vol. 47, pp. 427–480, 2009.
[3] P. Caselli, "Observational studies of pre-stellar cores and infrared dark clouds," *Proc. Int. Astron. Union*, vol. 7, no. S280, pp. 19–32, 2011.
[4] C. Ceccarelli *et al.*, "Herschel spectral surveys of star-forming regions-Overview of the 555–636 GHz range," *Astron. Astrophys.*, vol. 521, 2010, Art. no. L22.
[5] F. Combes and G. Pineau des Forêts, *Molecular Hydrogen in Space*. Cambridge, U.K.: Cambridge Univ. Press, 2001.
[6] R. Bouwens *et al.*, "UV continuum slope and dust obscuration from z∼6 to z∼2: The star formation rate density at high redshift," *Astrophys. J.*, vol. 705, no. 1, pp. 936–961, 2009.
[7] J. P. Williams and L. A. Cieza, "Protoplanetary disks and their evolution," *Annu. Rev. Astron. Astrophys.*, vol. 49, pp. 67–117, 2011.
[8] H. Hirashita *et al.*, "First-generation science cases for ground-based Tera-hertz telescopes," *Publ. Astron. Soc. Jpn.*, vol. 68, no. 1, pp. 27–28, 2016.

[9] C. Kulesa, "Terahertz spectroscopy for astronomy: From comets to cosmology," *IEEE Trans. THz Sci. Technol.*, vol. 1, no. 1, pp. 232–240, Sep. 2011.

[10] B. D. Jackson *et al.*, "Low-noise 0.8-0.96-and 0.96-1.12-THz superconductor-insulator-superconductor mixers for the Herschel Space Observatory," *IEEE Trans. Microw. Theory Techn.*, vol. 54, no. 2, pp. 547–558, Feb. 2006.

[11] T. Kojima *et al.*, "Three quanta sensitivity superconductor–insulator–superconductor mixer for the 0.78–0.95 THz band," *Appl. Phys. Exp.*, vol. 2, no. 10, 2009, Art. no. 102201.

[12] Y. Uzawa *et al.*, "Design of terahertz SIS mixers using Nb/AlN/Nb junctions integrated with all-NbTiN tuning circuits," *IEEE Trans. Appl. Supercond.*, vol. 27, no. 4, Jun. 2017, Art. no. 1500705.

[13] A. Karpov *et al.*, "Low noise 1 THz–1.4 THz mixers using Nb/Al-AlN/NbTiN SIS junctions," *IEEE Trans. Appl. Supercond.*, vol. 17, no. 2, pp. 343–346, Jun. 2007.

[14] A. Khudchenko *et al.*, "High-gap Nb-AlN-NbN SIS junctions for frequency band 790–950 GHz," *IEEE Trans. THz Sci. Technol.*, vol. 6, no. 1, pp. 127–132, Jan. 2016.

[15] B. Leone, B. Jackson, J. Gao, and T. Klapwijk, "Geometric heat trapping in niobium superconductor–insulator–superconductor mixers due to niobium titanium nitride leads," *Appl. Phys. Lett.*, vol. 76, no. 6, pp. 780–782, 2000.

[16] P. Dieleman, T. Klapwijk, S. Kovtonyuk, and H. van De Stadt, "Direct current heating in superconductor–insulator–superconductor tunnel devices for THz mixing applications," *Appl. Phys. Lett.*, vol. 69, no. 3, pp. 418–420, 1996.

[17] B. Leone *et al.*, "Hot electron effect in terahertz hybrid devices," *IEEE Trans. Appl. Supercond.*, vol. 11, no. 1, pp. 649–652, Mar. 2001.

[18] B. Tan, G. Yassin, P. Kittara, and J. Leech, "Measurement of electron-phonon interaction time of niobium using heating effect in SIS tunnel junction," in *Proc. 20th Int. Symp. Space THz Technol.*, 2009, pp. 1–2.

[19] M. Westig, S. Selig, K. Jacobs, T. Klapwijk, and C. Honingh, "Improved Nb SIS devices for heterodyne mixers between 700 GHz and 1.3 THz with NbTiN transmission lines using a normal metal energy relaxation layer," *J. Appl. Phys.*, vol. 114, no. 12, 2013, Art. no. 124504.

[20] S. Selig, M. P. Westig, K. Jacobs, M. Schultz, and N. Honingh, "Heat transfer coefficient saturation in superconducting Nb tunnel junctions contacted to a NbTiN circuit and an Au energy relaxation layer," *IEEE Trans. Appl. Supercond.*, vol. 25, no. 3, Jun. 2015, Art. no. 2400705.

[21] A. Baryshev *et al.*, "The ALMA Band 9 receiver—Design, construction, characterization, and first light," *Astron. Astrophys.*, vol. 577, 2015, Art. no. A129.

[22] B.-K. Tan *et al.*, "A high performance 700 GHz feed horn," *J. Infrared, Millimeter, Terahertz Waves*, vol. 33, no. 1, pp. 1–5, 2012.

[23] A. Hector, A. V. Trifonov, E. Tong, P. Grimes, and G. Yassin, "A smooth walled four pixel feed horn array operating at 1.4 THz," in *Proc. 28th Int. Symp. Space Terahertz Technol.*, 2017, pp. 1–3.

[24] K. Jacob, A. Schroder, and A. Murk, "Design, manufacturing, and characterisation of conical blackbody targets with optimized profile," *IEEE Trans. THz Sci. Technol.*, vol. 8, no. 1, pp. 76–84, Jan. 2018.

[25] H. B. Callen and T. A. Welton, "Irreversibility and generalized noise," *Phys. Rev.*, vol. 83, no. 1, pp. 34–40, 1951.

[26] A. Skalare, "Determining embedding circuit parameters from dc measurements on quasiparticle mixers," *Int. J. Infrared Millimeter Waves*, vol. 10, no. 11, pp. 1339–1353, 1989.

[27] M. Tinkham, *Introduction to Superconductivity*. Chelmsford, MA, USA: Courier Corporation, 2004.

[28] C.-Y. E. Tong, A. Hedden, and R. Blundell, "An empirical probe to the operation of SIS receivers? Revisiting the technique of intersecting lines," in *Proc. 19th Int. Symp. Space THz Technol.*, 2008, pp. 314–318.

Alessandro Traini received the bachelor's degree in physics from the University of Camerino, Camerino, Italy, in 2010, and the master's degree in physics and astrophysics from the University of Florence, Florence, Italy, in 2014, and the D.Phil. degree in astrophysics from the University of Paris Diderot, Paris, France, in 2018.

He is currently with the Department of Physics (Astrophysics), University of Oxford, Oxford, U.K.

Boon-Kok Tan received the B.Eng. degree in electrical and electronic engineering and the M.Eng. degree in solar engineering from the University of Technology Malaysia, Johor Bahru, Malaysia, in 2001 and 2003, respectively, and the D.Phil. degree in astrophysics from the University of Oxford, Oxford, U.K., in 2012.

He is currently with the Department of Physics (Astrophysics), University of Oxford. His current research interests include the development of ultra-sensitive millimeter and submillimeter detectors and terahertz components and broadband superconducting quantum amplifiers, for astronomy and quantum information technologies.

Dr. Tan was the recipient of the European Best Thesis Award by the European Astronomical Society in 2014.

John D. Garrett received the B.Sc. degree in electrical engineering from the University of Alberta, Edmonton, AB, Canada, in 2012, the M.Sc. degree in electrical engineering from the University of Calgary, Calgary, AB, Canada, in 2014, and the D.Phil. degree in astrophysics from the University of Oxford, Oxford, U.K., in 2018.

He is currently a Submillimeter Array Postdoctoral Fellow with the Harvard–Smithsonian Center for Astrophysics, Cambridge, MA, USA. His research interests include developing wide bandwidth superconductor–insulator–superconductor (SIS) mixers, focal plane arrays, and software for simulating SIS junctions.

Andrey Khudchenko received the M.S. degree in applied physics and mathematics and the Ph.D. degree in radiophysics from the Moscow Institute of Physics and Technology, Moscow, Russia, in 2007 and 2009, respectively.

Since 2009, he has been a Researcher with the Kotel'nikov Institute of Radio Engineering and Electronics, Moscow. From 2009 to 2015, he was an Instrument Scientist with The Netherlands Institute for Space Research SRON and from 2015 to 2020, an Instrument Scientist with the Kapteyn Astronomical Institute, University of Groningen, Groningen, The Netherlands. Since 2020, he has been with the Astro Space Center, Lebedev Physical Institute, Russian Academy of Science, Moscow. His main research interests include the development of new heterodyne terahertz instruments.

Ronald Hesper received the M.Sc. degree in experimental solid state physics from the University of Leiden, Leiden, The Netherlands, in 1994, and the Ph.D. degree in experimental solid state physics from the University of Groningen, Groningen, The Netherlands, in 2000.

Since 2000, he has been an Instrument Scientist with the Kapteyn Astronomical Institute, University of Groningen. From 2000 to 2008, he was involved in the technological development of the ALMA Band 9 receivers, including the process of industrialization, as well as related projects such as the CHAMP+ mixer arrays for APEX; from 2008 to 2013, on the development of a sideband-separating mixer upgrade for the ALMA Band 9 receivers; and from 2013 to the beginning of 2015, on the industrialization of the ALMA Band 5 receivers. He is currently working on the development of new (arrayable) sideband-separating heterodyne detector technologies at frequencies around 1 THz, as well as on the development and industrialization process of the ALMA Band 2 receivers.

Andrey M. Baryshev, photograph and biography not available at the time of publication.
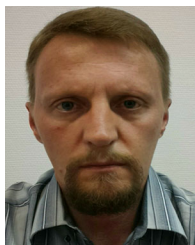
Pavel N. Dmitriev received the M.S. degree in material science from the Lomonosov Moscow State University of Fine Chemical Technologies, Moscow, Russia, in 1993, and the Ph.D. degree in development of superconductor–insulator–superconductor mixers from the Kotel'nikov Institute of Radio Engineering and Electronics, Russian Academy of Sciences, Moscow, in 1993.

He is currently with the Kotel'nikov Institute of Radio Engineering and Electronics, Russian Academy of Sciences. His research interests include development and fabrication of superconducting circuits.

Valery P. Koshelets received the M.S. degree in physics from the Lomonosov Moscow State University, Moscow, Russia, in 1973, and the Ph.D. degree in radio physics and the Doctor of Sciences (Habilitation) degree in physical electronics from the Kotel'nikov Institute of Radio Engineering and Electronics, Russian Academy of Sciences, Moscow, in 1978 and 1990, respectively.

Since 1973, he has been with the Kotel'nikov Institute of Radio Engineering and Electronics, Russian Academy of Sciences, where he is currently the Head of the Laboratory of Superconducting Devices for Signal Detection and Processing.

Ghassan Yassin, photograph and biography not available at the time of publication.